Computation of Normal Shocks Running into a Cloud of Particles using a High-Order Particle-Source-in-Cell Method.

G. B. Jacobs *

Department of Aerospace Engineering & Engineering Mechanics, San Diego State University, San Diego, CA, 92182.

W. S. Don †

Department of Mathematics, Hong Kong Baptist University, Hong Kong, China.

T. Dittmann ‡

Department of Aerospace Engineering & Engineering Mechanics, San Diego State University, San Diego, CA, 92182.

In this paper, the two-dimensional particle-laden flow developments are studied with bronze particle cloud in the accelerated flow behind a running shock. The forty thousands particle clouds are arranged initially in a rectangular, triangular and circular shape. The flows are computed with a recently developed high-order Eulerian-Lagrangian method, that approximates the Euler equations governing the gas dynamics with the improved high order weighted essentially non-oscillatory (WENO-Z) scheme, while individual particles are traced in the Lagrangian frame using high-order time integration schemes. A high-order ENO interpolation determines the carrier phase properties at the particle location. A high-order central weighing deposits the particle influence on the carrier phase. Reflected shocks form ahead of all the cloud shapes. The detached shock in front of the triangular cloud is weakest. At later times the wake behind the cloud becomes unstable and a two-dimensional vortex-dominated wake forms. Separated shear layers at the edges of the clouds pulls particles initially out of the clouds that are consequently transported along the shear layers. Since flows separated trivially at sharp corners, particles are mostly transported out of the cloud into the flow at the sharp front corner of the rectangular cloud, and the trailing corner of the triangular cloud. Particles are transported smoothly out of the circular cloud, since it lacks sharp corners. At late times, the accelerated flow behind the running shock disperses the particles in cross-stream direction the most for the circular cloud, followed by the rectangular cloud and the triangular cloud.

I. Introduction

Shock waves are encountered in many technological environments, like supersonic aircraft, hypersonic space vehicles, jet engines, and explosions. Often the flow containing shocks interact with solid or liquid particles. For example, liquid or solid fuel particles interact with a chemically reacting fluid containing shock waves in high speed combustors. Debris interacts with shocks and fluid turbulence in dust explosions. In lithotripsy, kidney stones are broken into smaller kidney stone particles by means of shocks. When the flow containing shocks is turbulent, the scale range of the gas dynamics is enormous. The mutual exchange of mass, momentum and energy of particles and the carrier gas results in even more complex, multi-scale physics. The complexity and size of the particle-laden shock flow problems has left many open problems.

The direct analysis of the particle-laden shocked flow requires the computation of the complete flow over each particle, the tracking of individual solid or liquid complex particle boundaries along their paths, and the tracking of shock waves in the moving framework. The individual computational components are

*Assistant Professor, AIAA member, Email: gjacobs@mail.sdsu.edu
†Professor, Email: wsdon@math.hkbu.edu.hk
‡Graduate Student

difficult to resolve and currently barely within reach even with the advances of computational technologies. The combined problem of shock and particles has an immense complexity, scale range and size, that can currently potentially be analyzed in highly idealized situation with a few particles.

Simplified models are required to handle more realistic situations. Eulerian-Lagrangian (EL) methods have provided outcome for particle-laden flows. In particular, EL methods that model particles as points like the Particle-Source-in-Cell (PSIC) method.[1] In PSIC the carrier gas is solved in the Eulerian frame on a mesh, while individual particles are modeled as points and are traced along their path in a Lagrangian formulation. The carrier gas and the particles are coupled through interpolation. The point modeling of particles enables the computation of a large, realistic number of particles and simulation of particle-laden flow in engineering applications.

The main difficulty in shock capturing and tracing is to accurately capture the sharp discontinuous shock jump in the flows fields in a stable manner. Often times, robustness considerations lead to a preference for low order methods that have excessive numerical diffusion near the shock. Even though, this is often good enough to capture the short time dynamics of the shock, the numerical diffusion dissipates important smaller scale flow structures in the wake of the shock. Moreover, long time capturing of the shock is inaccurate. The particle-mesh method also typically relies on relatively simple, coarse grids and/or numerical schemes with low order of accuracy, i.e. first order or second order methods. Lower order based methods limit the accurate computation of particle-laden flows with a large range of active temporally and spatial scales. Dispersion and diffusion errors plague the accuracy of the solution.

For problems in which a large number of ranges coexist, high order and high resolution numerical algorithms have great potential to accurately and efficiently capture all flow features for long time. In Ref. 2, we initiated the development of a high-order algorithm PSIC algorithm for the computation of particle-laden flow of shocks. We solved the gas dynamics with an improved high order Weighted Essentially Non-Oscillatory schemes (WENO-Z).[3] This type of method has proven very effective for the simulation of the fine scale and delicate structures of the physical phenomena involving shocks. A consistent and stable high-order ENO interpolation was introduced for interpolation of the gas flow to the particle. A smooth higher ordering weighing ensured a low noise and accurate coupling of the particles to the gas. Time integration of the carrier phase and the particles is performed with a high order Runge-Kutta TVD method without splitting.

In this paper, we compare the computed particle-laden flow developments of several cloud shapes of bronze particles initially seeded in the accelerated flow behind a running shock using our high-order PSIC method. We compare three initial cloud shapes including a rectangular, a circular and a triangular shape. Boiko et al.[4] and Kiselev et al.[5] have reported on the flow development with rectangular cloud shape. Their computations revealed particle transport mechanisms and flow developments. They also partially validated their computations with experiments in a shock tube. In Ref. 2 we revisited this flow using the high-order PSIC method. It was shown that the high-order method is more able than low-order methods to simultaneously capture the shock and small scale flow developments in the wake of the cloud. Analysis of the rectangular cloud revealed that at long times particles accumulate in the particle streaks that form from the corners of the rectangular shape. Here, we compare the particle-laden flow of the initial rectangular cloud with developments of an initially circular and triangular particle cloud. We show that the change of initial shape dramatically changes the dispersion of the particles at early and late times. Detonation type shock waves will have the largest impact on the circular cloud shape, while the triangular cloud shape is least affected by the accelerated flow behind a running shock.

We will briefly review the developed high order PSIC method followed by a discussion of a moving shock interacting with a cloud of particles that have three different initial shapes including a rectangle, a triangle and a circle. In section II, the PSIC formulation is presented. We give a brief description of the improved fifth order weighted essentially non-oscillatory scheme WENO-Z. We summarize the high order particle algorithm, including interpolation, weighing and time integration. In Section III, we discuss the two dimensional shock-particles cloud interactions computed with the high-order PSIC method. Conclusion and direction of future research are given in Section IV.

II. The Physical Model and Particle-Source-In-Cell method

In the particle-source-in-cell (PSIC) method the Eulerian continuum equations are solved for the carrier flow in the Eulerian frame, while particles are traced along in the Lagrangian frame.

In the following, we shall denote the subscript p for the particle variables and f for the gas variables at the particle position. Variables without subscript refer to the gas variables unless specified otherwise.

A. Euler equation in the Eulerian frame

The governing equations for the carrier flow are the two-dimensional Euler equations in Cartesian coordinates given by:

$$\mathbf{Q}_t + \mathbf{F}_x + \mathbf{G}_y = \mathbf{S}, \tag{1}$$

where

$$\begin{aligned} \mathbf{Q} &= (\rho, \rho u, \rho v, E)^T, \\ \mathbf{F} &= \left(\rho u, \rho u^2 + P, \rho uv, (E+P)u\right)^T, \\ \mathbf{G} &= \left(\rho v, \rho uv, \rho v^2 + P, (E+P)v\right)^T, \end{aligned} \tag{2}$$

and the equation of state is

$$P = (\gamma - 1)\left(E - \frac{1}{2}\rho\left(u^2+v^2\right)\right), \qquad \gamma = 1.4 \tag{3}$$

$$T = \frac{\gamma P M^2}{\rho}, \tag{4}$$

where $M = U/\sqrt{\gamma R T}$ is a reference Mach number determined with the reference velocity, U and reference temperature, T. The source term, $\mathbf{S}$, accounts for the effect of the particles on the carrier gas and will be discussed in more detail below.

B. Particle equation in the Lagrangian frame

Particles are tracked individually in the Lagrangian frame. The kinematic equation describing the particle's position $\vec{x}_p$, is given as

$$\frac{d\vec{x}_p}{dt} = \vec{v}_p, \tag{5}$$

where $\vec{v}_p$ is the particle velocity vector.

The particles' acceleration is governed by Newton's second law forced by the drag on the particle. With particles assumed spherical, we take the drag as a combination of the Stokes drag corrected for high Reynolds and Mach number and the pressure drag leading to the following equations governing the particle velocity,[4]

$$\frac{d\vec{v}_p}{dt} = f_1\left(\frac{\vec{v}_f - \vec{v}_p}{\tau_p}\right) - \frac{1}{\rho_p}\boldsymbol{\nabla} P|_f, \tag{6}$$

where $\vec{v}_f$ is the velocity of the gas at the particle position, ρ_p the particle density. The first term on the right hand side describes the particle acceleration resulting from the velocity difference between the particle and the gas. f_1 is an empirical correction factor[4] that yields an accurate determination within 10% of measured particle acceleration for higher relative particle Reynolds number up to $Re_f = 10,000$ and relative particle Mach number up to $M_f = |\vec{v}_f|/\sqrt{T_f} = 1.2$ and is given by

$$f_1 = \frac{3}{4}\left(24 + 0.38 Re_f + 4\sqrt{Re_f}\right)\left(1 + \exp\left[\frac{-0.43}{M_f^{4.67}}\right]\right). \tag{7}$$

The second term is the particle acceleration induced by the pressure gradient in the carrier flow at the particle position. The particle time constant $\tau_p = Re d_p^2 \rho_p/18.0$, where d_p is the particle diameter, is a measure for the reaction time of the particle to the changes in the carrier gas. $Re = UL/\nu$ is the Reynolds number of the carrier gas flow with L a reference length and ν the dynamic viscosity. Here, we assume Re large and we therefore do not model viscous effects in the governing Eulerian equations for the gas flow (1).

The particle temperature is mostly affected by convection. From the first law of thermodynamics and Fourier's law for heat transfer, the equation for temperature is derived as,

$$\frac{dT_p}{dt} = \frac{1}{3}\frac{Nu}{Pr}\left(\frac{T_f - T_p}{\tau_p}\right), \tag{8}$$

where $Pr = 1.4$ is the Prandtl number, taken as its typical value for air in this paper. $Nu = 2 + \sqrt{Re_f}Pr^{0.33}$ is the Nusselt number corrected for high Reynolds number.

C. Source term S for the Euler equation

Each particle generates a momentum and energy that affects the carrier flow. The volume averaged summation of all these contributions gives a continuum source contribution on the momentum and energy equation in (1) as:

$$\vec{S}_m(\vec{x}) = \sum_{i=1}^{N_p} \mathbf{K}(\vec{x}_p, \vec{x}) \vec{W}_m, \tag{9}$$

$$S_e(\vec{x}) = \sum_{i=1}^{N_p} \mathbf{K}(\vec{x}_p, \vec{x})(\vec{W}_m \cdot \vec{v}_p + W_e), \tag{10}$$

where $\mathbf{K}(x, y) = \mathbf{K}(|x - y|)/V$ is a normalized weighing function that distributes the influence of each particle onto the carrier flow. $\vec{W}_m = m_p f_1(\vec{v}_f - \vec{v}_p)/\tau_p$ and $W_e = m_p(Nu/3Pr)\,(T - T_p)\,/\tau_p$ are weigh functions describing the momentum and energy contribution of one particle, respectively. m_p is the mass of one spherical particle which can be derived from τ_p. N_p is the total number of particles in an finite volume V. The normalized weighing function will be further discussed below.

D. Flow solver

The carrier flow equations (1) are discretized spatially with a fifth-order weighted essentially non-oscillatory conservative finite difference scheme (WENO-Z)[6] in a uniform mesh and temporally with the third order Runge-Kutta TVD scheme.

The nonlinear nature of the hyperbolic Euler equations admits finite time singularities in the solution even when the initial condition is smooth. It is important that the numerical methods employed avoid non-physical oscillations, also known as the Gibbs phenomenon, when the solution becomes discontinuous. Among many high order shock capturing schemes, the weighted essentially non-oscillatory finite difference schemes (WENO) for conservation laws[7] has been very successfully employed for the simulation of the fine scale and delicate structures of the physical phenomena related to shock-turbulence interactions.

The essence of the WENO scheme is the nonlinear adaptive stencils, where a nonlinear convex combination of lower order polynomials adapts either to a higher order approximation at smooth parts of the solution, or to an upwind lower order spatial discretization that avoids interpolation across discontinuities and provides the necessary dissipation for shock capturing. The nonlinear coefficients of the convex combination, hereafter referred to as classical weights, are based on the local smoothness indicators, which measure the sum of the normalized squares of the scaled L^2 norms of all derivatives of the lower order polynomials. An essentially zero weight is assigned to those lower order polynomials whose underlining stencils contains high gradients and/or shocks, yielding an essentially non-oscillatory solution at discontinuities. At smooth regions, higher order is achieved through the mimicking of the central upwinding scheme of maximum order, when all the smoothness indicators are about the same size. The classical weights were later further improved by Costa et al. that made use of existing higher order information contained within the stencils. The improved weights[6] (WENO-Z) were shown to satisfy the necessary and sufficient conditions for the optimal order of the given fifth order scheme.

At each grid point, the first order Lax-Friedrichs flux splitting is used as the low order building block to split the Euler flux, ignoring the source term, into the positive and negative going fluxes. The positive and negative going fluxes are then decomposed into the characteristic variables via the left eigenvectors and eigenvalues of the Euler flux. The eigensystem of the Euler flux is obtained via the linearized Riemann solver of Roe.[8] The characteristic variables are then reconstructed via the improved high order weighted essentially non-oscillatory (WENO-Z) scheme as discussed above. The reconstructed characteristic variables are then re-projected back into the physical space as the numerical flux via the right eigenvectors (see Shu et al.[7] for further details.)

E. Particle solver

Lagrangian tracking of the particles consists of three stages per particle, including searching the element a particle is located in, interpolating the field variables to the particle location, and pushing the particle forward with a time integration method.

Locating the host cell of a particle is a trivial task on a structured grid. Following Jacobs and Hesthaven,[10] to avoid aliasing errors and an unphysical numerical total energy increase, the order of interpolation has to equal the approximation order k of the stencil S_k and the time integration of the particle solver and the carrier phase solver have to match. To determine the field variables at the particle location we use the ENO interpolation introduced by Jacobs and Don[2] suited to flows containing shock discontinuities. The ENO interpolation was shown to prevent Gibbs oscillations plague the accuracy of the centered interpolation over shocks.

In smooth flow areas without shocks, the WENO-Z method uses a central difference scheme. A centered interpolation to the particle position is then most accurate and preferred. We use Lagrange interpolating polynomial of degree k,

$$\mathbf{P}_k(x_p) = \sum_{i=i_p-k/2}^{i_p+k/2} \mathbf{Q}(x_i) l_i(x_p), \tag{11}$$

where i_p represents the nearest cell center to the left of the particle position. The number of points k should be equal to the number of points used as the order of the WENO scheme.[10] In the case of the fifth order WENO scheme, $k = 5$.

In shocked regions the centered interpolation will produce undesirable Gibbs oscillations. With an ENO interpolation,[13] these oscillations are essentially removed. ENO interpolation is only necessary in WENO-domains identified by the smoothness indicator. In those domains, the interpolating points are determined based on smoothness of the function indicated by the divided differences. The k-th degreed divided differences are determined first.

The 0-th order divided differences of Q are defined by:

$$Q[x_i] \equiv Q(x_i). \tag{12}$$

The j-th degree divided difference for $j \geq 1$ are defined by

$$Q[x_i, \cdots, x_{i+j}] \equiv \frac{Q[x_{i+1}, \cdots, x_{i+j}] - Q[x_i, \cdots, x_{i+j-1}]}{x_{i+j} - x_i}. \tag{13}$$

Starting from a two point stencil , x_{i_p}, x_{i_p+1}, the interpolation stencil is expanded to k points based on a comparison of the divided differences of the the increasing order at i_p. The smallest second order divided differences at i_p of the two potential three point stencils $\min\left\{Q[x_{i_p-1}, x_{i_p}, x_{i_p+1}], Q[x_{i_p}, x_{i_p+1}, x_{i_p+2}\right\}$ indicates the smoothest interpolation stencil and is therefore chosen. This procedure is repeated until a k point interpolant is found. The Lagrange interpolant in (11) then interpolates to the particle position.

In two dimensions, the same procedure can be used along the separate dimension on the tensor grid. The divided differences are determined along horizontal and vertical lines in the grid. With the 1D approach outline above, we find the left most and bottom most grid point of the interpolation stencil with $k \times k$ points for each grid point in the domain.

We give an example of a two dimensional ENO stencil in Fig. 1. The particle's nearest grid point is found to the bottom, left of the particle. The left and bottom point of the ENO stencil are determined by comparison of the divided difference along the horizontal and vertical line crossing the nearest grid point. If a particle is located in a cell with a shock, then the ENO is one-sided to the left and bottom of the particle. We note that if two shocks cross the k interpolation stencil, then this procedure will fail to recognize the second shock. This is, however, mostly a rare short-lived event. We did not encounter stability problems in the simulations we performed below.

To determine the particle influence on the carrier flow (10), we use the high-order spline interpolation discussed in Ref. 12. The high-order weighing reduces aliasing and noise in the sources (10) that couple the particles to the gas flow. The spline S_k is constructed by the convolution of the square nearest-grid-point or zero order weighting function. For large k the spline approaches the Gaussian function. The 0_th mode of function in wave space is free of aliasing errors, and the higher component of the function in wave space are smaller than equivalent Lagrangian interpolations.

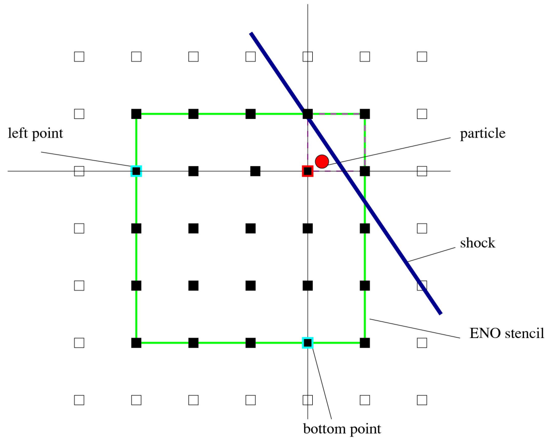

Figure 1. Two dimensional ENO stencil for interpolation to a particle located near to a shock. The left and bottom point of the interpolation stencil is determined based on the divided differences along the horizontal grid lines and the vertical grid lines at the particle's nearest grid point to the left and bottom of the particle.

III. Rectangular, Circular and Triangular Particle Cloud in the Accelerated Flow Behind a Running Shock

In Ref. 2 we revisited the interaction of a running shock with a cloud of bronze particles in 1D and 2D studied by Boiko et al.[4] and Kiselev et al.[5] We demonstrated that the high order PSIC method improved the capturing of the small scale flow structures behind the running shock, while the global features compared well to the computations and experiments by Boiko and Kiselev. We also discussed the long time particle dispersion of an initial rectangular cloud shape in the accelerated flow behind a shock.

Here, we present additional results of the bronze particle dynamics of an initially triangular and circular cloud shape in the accelerated flow behind a shock. All cloud shapes cover a same area and are initiated with the same number of particles with the same mass leading to comparable initial particle number densities.

For all cases, we initialize a right running shock with $M_s = 3$ at $x_s = 0.175$ in a rectangular domain $[0, 3] \times [-0.611, 0.611]$. The state of the pre-shock flow is

$$[\rho_R, u_R, p_R] = [1, 0, 1]. \quad (14)$$

The post-shock state can be computed via the well-known Rankine-Hugoniot relations for a given Mach number M_s. Free stream inflow and outflow boundary conditions are imposed in the inflow and outflow boundaries, respectively, in the x direction. A periodical boundary condition is imposed in the y direction. The cloud is seeded directly before the shock at time, $t = 0$ (e.g. see Fig. 2 for a circular cloud)

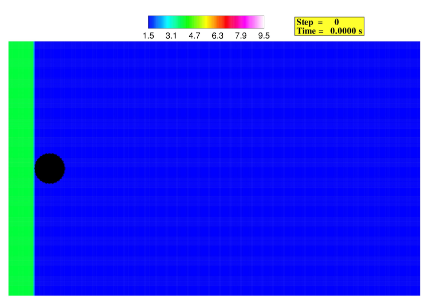

Figure 2. Initialization of a circular cloud of particles directly before the right running shock visualized by the density contours at time $t = 0$.

A. Initialization of particle clouds

The rectangular cloud is seeded with uniformly distributed particles at $[0.175, 0.352] \times [0.044, 0.044]$ with zero initial velocity. The circle is initialed with a radius of 0.0704 yielding the same surface area as the rectangle. The circle center is at [0.2454,0]. For the initial triangle to cover the same surface area as the rectangle and the circle, the height of the triangle has to be 0.176. The volume concentration of the particles in all cloud shapes is four percent. The particle response time and density are, $\tau_p = 51.69$ and $\rho_p = 7.42 \times 10^4$, respectively, corresponding to an experiment with bronze particles in Ref. 5. We take the Reynolds number needed to compute the particle traces according to the experiment at $Re_f = 3.387 \times 10^7$.

B. Particle-Laden Flow Development at Early Time

We discuss the particle-laden flow development through snapshots of the vorticity and the particles at four non-dimensional times of $t = 0.1$, 0.225, 0.5, 0.75 in Figs. 3, 4, and 5. The vorticity magnitude $|\omega|$ is plotted in the left column, and the trajectory of the particles in the right column. A dotted rectangle, circle and triangle in the figures shows the original shape and position of the particles at $t = 0$ for reference.

The overall flow field maintains its symmetry at early times up to $t = 0.225$. At later times the wake behind the cloud is unstable.

When the right running shocks hits the particle cloud, a reflected shock forms at the front end of the cloud for each cloud shape. This shock development as visualized by the vorticity magnitude generated by the shock is comparable for the rectangular and circular shape. In both cases, a strong detached "bow" curved shock forms with a large part of the shock normal to the flow, as typical for blunt objects. The bow shock moves upstream at comparable velocity from $t = 0.1$ to $t = 0.225$ for the rectangle and circle. At the sharp front corner of the triangle the reflected shock, however, stays attached until $t = 0.1$ and does not move significantly upstream throughout the flow development.

The right running shock moves along the top and bottom sides of the clouds and has passed the cloud at time $t = 0.1$. The refracted shock is curved towards the symmetry line at $y = 0$. Since the triangle is wider at the back end and hence the distance to the symmetry line larger, the curvature of the right shock is larger for the triangle as compared to the other two cases.

At early times the particle clouds act like solid bodies in gas flow. The interaction of the accelerated flow with the particle cloud leads to an increased vorticity near the cloud. At sharp edges the flow separates from the cloud. The flow separates at the front corners of the rectangular shape. The shear layer reattaches to the cloud further downstream and separates again at the trailing edge. In the triangle cases, a shear layer separates only at the sharp trailing edge. The circle has no sharp edge, and the separation location moves forward from time $t = 0.1$ to $t = 0.225$.

The separated shear layer is strongly correlated to the transport of particles out of the cloud into the flow at early times. The strong vorticity in the separated shear zones pulls the particles out of the shape, hence, forming the distinct arms and legs previously observed for the rectangle,[2] and the two particle streaks at the rear of the triangle shape. Since the shear layer moves for the circle shape case, the particle streaks out of the shape are less sharp as for the other two cases.

The accelerated flow stagnates at the front of the blunt rectangular and circular cloud shapes and compresses these clouds. The particles at the front end move towards the right at this early time and increase the particle density. The sharp edge of triangle yields a much lesser compression and the front location of the triangle has not moved towards the right as far as for the other two cases at $t = 0.225$. The sides of the triangle, however, are pushed more inward toward the symmetry line. The rectangle shape is also slightly compressed inward by the reattached flow on the top and bottom sides toward the symmetry line at $y = 0$.

In the wake of the shapes, initially two typical recirculation zones form that stretch in flow direction from $t = 0.1$ to $t = 0.225$. The reduced pressure and negative flow velocity push the rear edge of the particle cloud perhaps counter intuitively upstream.

C. Particle-Laden Flow Development at Late Time

The wake behind all shapes becomes unstable and loses its symmetry at later time (See Figures for $t = 0.5$ and $t = 0.75$). An asymmetric shedding is observed in the vorticity contour. Increasingly more particles have dispersed out of the cloud and the initial shape is hardly recognizable at later times.

The particles have mostly compressed or have formed long and thicker particle streaks into the main flow originating from the initial shape.

For the rectangle case, most particles are transported in the arm that forms at the front corner of the rectangle. The flow separation at the front corners and hence the particle streak emanating from the front corners persist throughout the computed interval. The particle arm shields the wake flow from the rear of the rectangular shape. This results in low flow velocities at the rear stagnating the transport of particles into the legs at the rear at later times.

A separated shear layer also persists for the circle case at later times, yielding a continuous transport of particles in the particle streak. Initially particles are drawn from the front half of the circle. Later on the front half of the circle is compressed in streamwise direction, and flow that accelerates to the right encounters the wider rear half of the circle that was initially pushed upstream by the recirculation behind the circle. The rear half of the circle induces a new shear layer at time $t = 0.5$ that widens the influence of the particle cloud on the flow as seen through the larger cross-stream dispersion and wider wake at $t = 0.75$ as compared to $t = 0.5$. The particle-laden wake of the circle is approximately fifty percent wider than the rectangle particle-laden wake.

The wake from the triangle cloud shape is significantly narrower than the rectangle and circle. At later times the front edge of the triangle has been compressed into a blunt nose. Two new particle streaks form off the front corners of this blunt following the separated shear layers in a comparable fashion to the case of the rectangle cloud shape. These new streaks reach further into the flow shielding the streaks at the rear end, that are further compressed toward the symmetry line.

IV. Conclusions and Future Developments

We have compared the computationally determined particle-laden flow developments of an initially rectangular, triangular and circular cloud of bronze particles in the accelerated flow behind a running (detonation) shock. We have used our recently developed Eulerian-Lagrangian method characterized by high-order resolution that is particularly capable of capturing shocks and the small scale particle-laden flow features in the accelerated flow behind the shock.

At early times particles are transported out of the initial shape following the separated shear flows from the shape. The flow separates trivially at the sharp corners of the rectangular and triangular cloud shape, leading to sharp particle streaks emanating from the clouds at these locations. The separation location is non-trivial and unsteady in case of the circular cloud shape and moves upstream at early times. Particles are transported into the flow from different locations of the shape at different times and hence form a particle streak that is less sharp.

The particle-laden wake is widest and particles are dispersed most in cross-stream, for the initially circular cloud shape, while the particle-laden wake is narrowest for the triangular shape despite it being the widest shape initially. The primary reason for the narrow wake is that particles are only moving out of the shape towards the symmetry line following the separated shear layer at the *rear* of the triangle that curves inward toward the symmetry line. No separation occurs at the front of the triangle, since the reflected shock at the front of the trianguler cloud is attached and weaker as compared to the shock reflected in the blunt circular and rectangular cloud. The flow also remains attached along the front edges of the triangle. The rectangle and circle both have a separated shear layers at the front of the shape that move away from the center symmetry lines and hence widen the wake area. The particle-laden wake of the circular cloud is wider than the rectangle, since a secondary separated shear layer away from the symmetry line is induced by the back half of the circle when the front half of the circle is compressed into the cloud by the accelerated flow.

We are currently characterizing the particle-laden flow developments of several particle cloud shapes and particle materials in the accelerated flow behind running shocks and will report on the complete characterization of the particle-laden flow developments when a shock hits a cloud of particles at rest in the near future.

V. Acknowledgments

The first author acknowledges the support of this work by AFOSR through a grant in the Young Investigator Program and by the University Grants Program at San Diego State University. The second author Don gratefully acknowledge the support of this work by the DOE under contract number DE-FG02-98ER25346 and the AFOSR under contract number FA9550-05-1-0123. The second author Don also would like to thank the support provided by the Department of Mathematics at Hong Kong Baptist University during his visit.

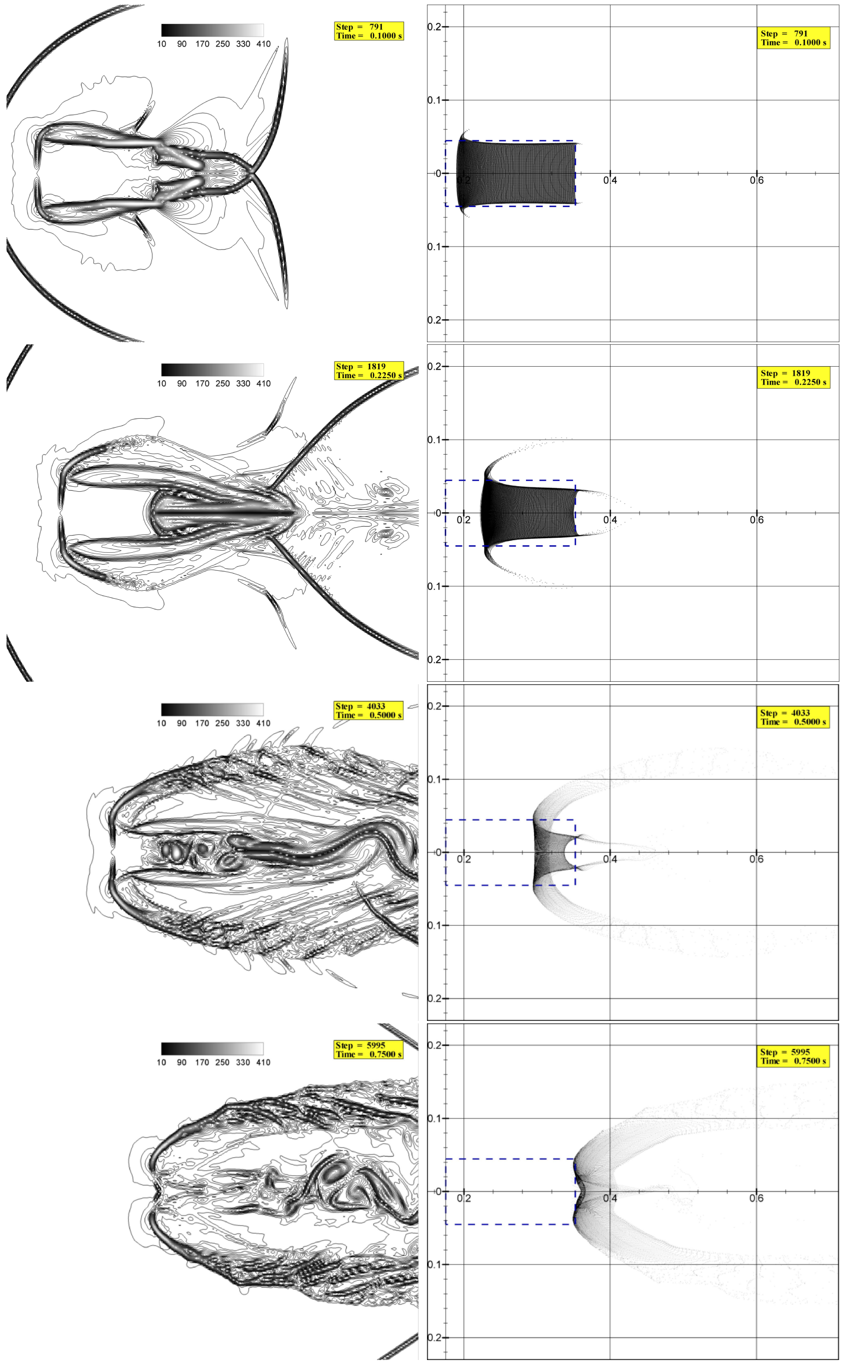

Vorticity $|\omega|$ Particle's Trajectory

Figure 3. A snapshot of the vorticity magnitude $|\omega|$ (left column) and the trajectory of the particle clouds (right column) for time $t = 0.1$, 0.225, 0.5, 0.75 (from top to bottom) as computed by the fifth order WENO-Z/PSIC-5 method with ENO interpolation scheme. The dotted rectangle in the figures showed the original shape and position of the particle clouds at $t = 0$ for easy reference. The shock Mach number is $M_s = 3$. The number of grid points used in the Eulerian frame is 1500×500 in the x and y directions respectively. The total number of bronze particle clouds is 40K.

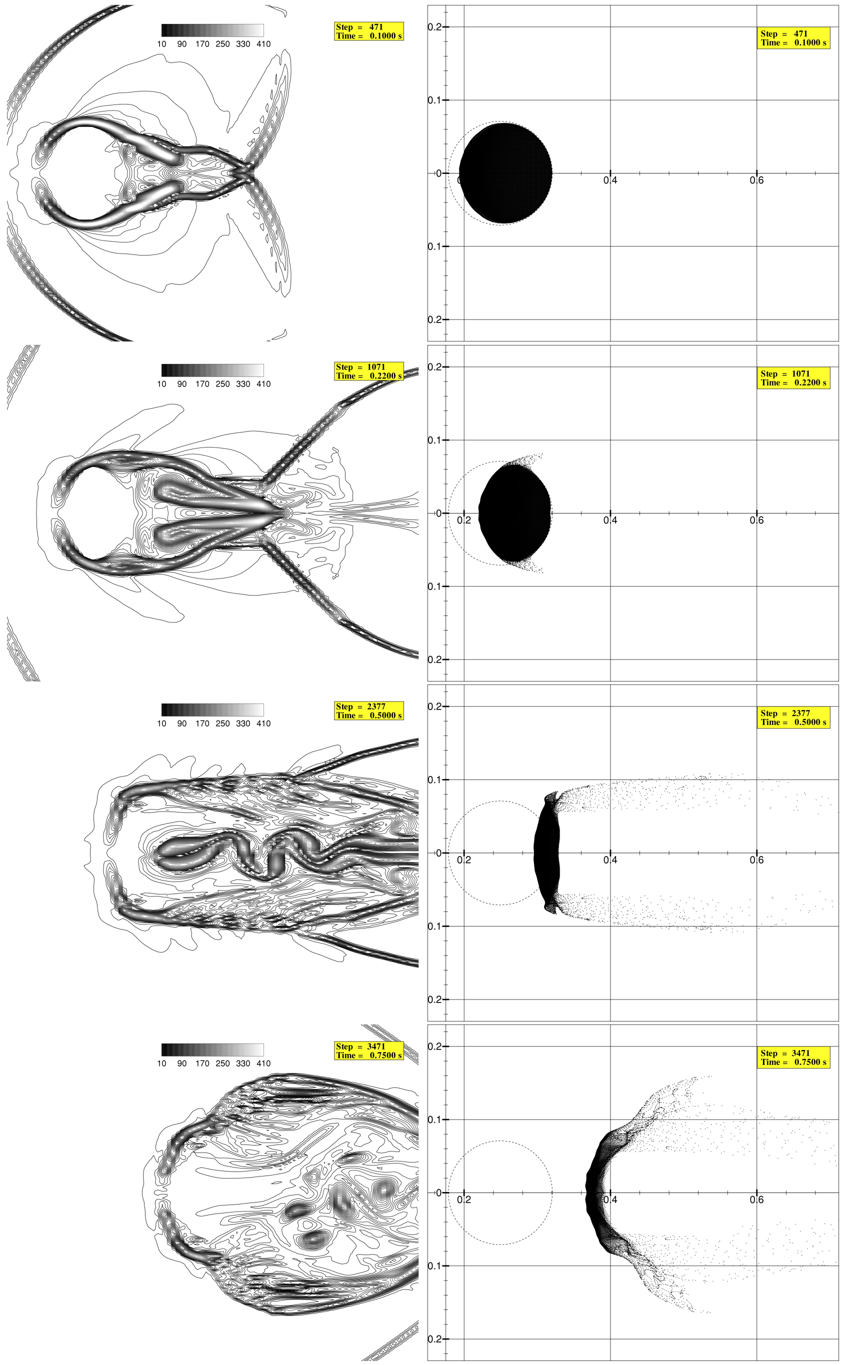

Vorticity $|\omega|$ Particle's Trajectory

Figure 4. A snapshot of the vorticity magnitude $|\omega|$ (left column) and the trajectory of the particle clouds (right column) for time $t = 0.1$, 0.225, 0.5, 0.75 (from top to bottom) as computed by the fifth order WENO-Z/PSIC-5 method with ENO interpolation scheme. The dotted triangle in the figures showed the original shape and position of the particle clouds at $t = 0$ for easy reference. The shock Mach number is $M_s = 3$. The number of grid points used in the Eulerian frame is 1500×500 in the x and y directions respectively. The total number of bronze particle clouds is 40K.

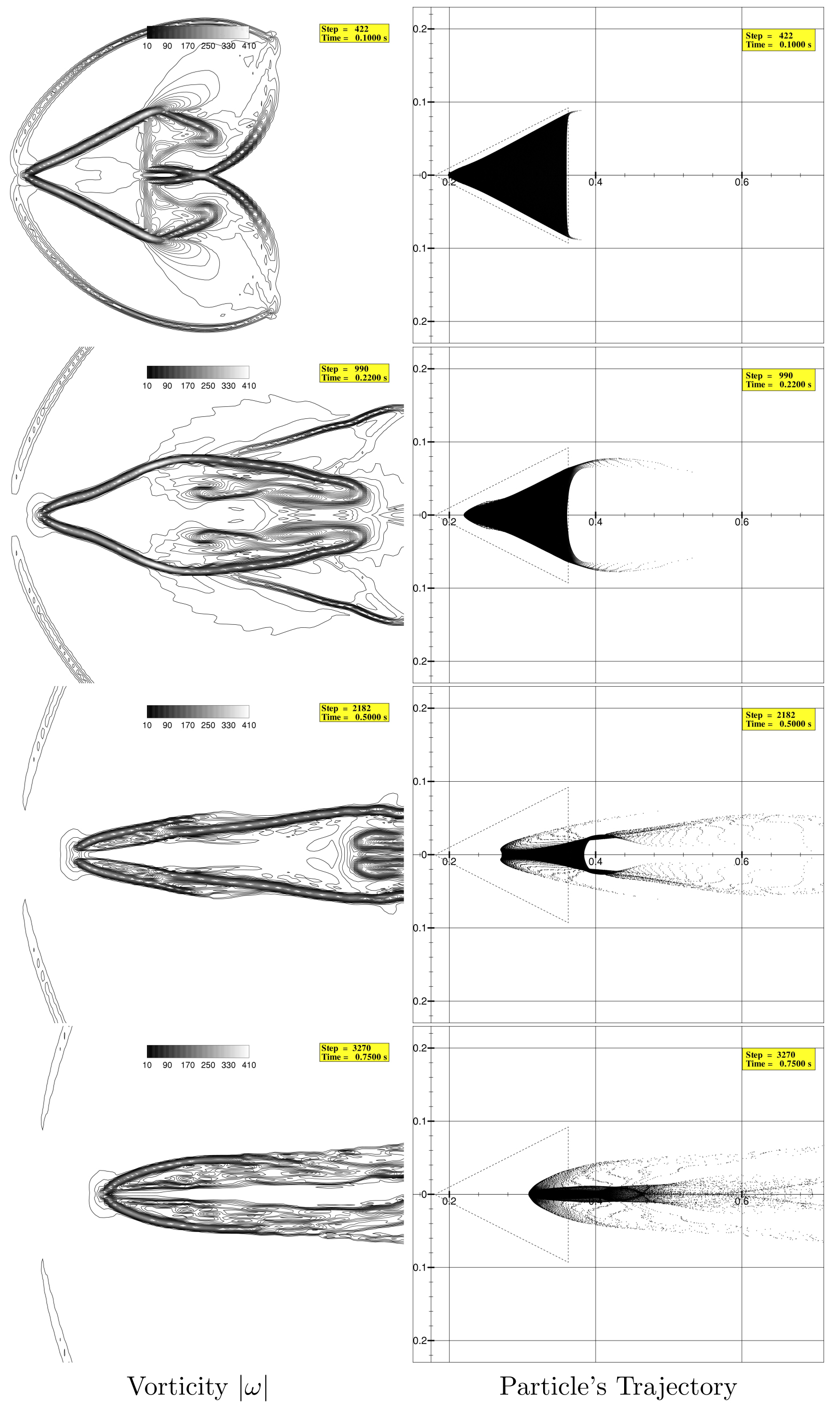

Figure 5. A snapshot of the vorticity magnitude $|\omega|$ (left column) and the trajectory of the particle clouds (right column) for time $t = 0.1$, 0.225, 0.5, 0.75 (from top to bottom) as computed by the fifth order WENO-Z/PSIC-5 method with ENO interpolation scheme. The dotted triangle in the figures showed the original shape and position of the particle clouds at $t = 0$ for easy reference. The shock Mach number is $M_s = 3$. The number of grid points used in the Eulerian frame is 1500×500 in the x and y directions respectively. The total number of bronze particle clouds is 40K.

References

[1] Crowe, C. T., Sharma, M. P., and Stock, D. E., "The Particle-Source in Cell (PSI-Cell) model for gas-droplet flows," *J. Fluids Eng.*, Vol. 6, 1977, pp. 325–332.

[2] Jacobs, G. and Don, W., "A high order WENO-Z finite difference methods based Particle-Source-in-Cell method for computaion of particle-laden flows with shock," *J. Comp. Phys.*, 2008. in press.

[3] Balsara, D. and Shu, C., "Monotonicity preserving weighted essentially non-oscillatory schemes with increasingly high order of accuracy," *J. Comp. Phys.*, Vol. 160, 2000, pp. 405–452.

[4] Boiko, V., Kiselev, V., Kiselev, S., Papyrin, A., Poplavsky, S., and Fomin, V., "Shock wave interaction with a cloud of particles," *Shock Waves*, Vol. 7, 1997, pp. 275–285.

[5] Kiselev, V., Kiselev, S., and Vorozhtsov, E., "Interaction of shock wave a particle cloud of finite size," *Shock Waves*, Vol. 16, 2006, pp. 53–64.

[6] Borges, R., Carmona, M., Costa, B., and Don, W., "An improved weighted essentially non-oscillatory scheme for hyperbolic conservation laws," *J. Comp. Phys.*, Vol. 227, 2008, pp. 3101–3211.

[7] Jiang, G. and Shu, C., "Efficient Implementation of Weighted ENO Schemes," *J. Comp. Phys.*, Vol. 126, 1996, pp. 202–228.

[8] Roe, P. L., "Approximate Riemann solvers, parameter vectors, and difference schemes," *J. Comp. Phys.*, Vol. 43, 1981, pp. 357–372.

[9] Jacobs, G. B., Kopriva, D. A., and Mashayek, F., "Towards efficient tracking of inertial particles with high-order multidomain methods," *J. Comp. Appl. Math.*, Vol. 206, 2007, pp. 392–408.

[10] Jacobs, G. B. and Hesthaven, J. S., "High-order nodal discontinuous Galerkin particle-in-cell method on unstructured grids," *J. Comp. Phys.*, Vol. 214, 2006, pp. 96–121.

[11] Birdsall, C. K. and Langdon, A. B., *Plasma physics via computer simulation.* McGraw-Hill, Inc., 1985.

[12] Abe, H., Natsuhiko, S., and Itatani, R., "High-order spline interpolations in the particle simulation," *J. Comp. Phys.*, Vol. 63, 1986, pp. 247–267.

[13] Shu, C.-W., "Essentially non-oscillatory and weighted essentially non-osillatory schemes for hyperbolic conservation laws," ICASE Report 97-65, NASA Langley Research Center, Hampton, VA, 1997.

[14] Maxey, M. R., Patel, B. K., and Wang, L., "Simulations of dispersed turbulent multiphase flow," *Fluid Dyn. Res.*, Vol. 20, 1997, pp. 143–156.